Bulk and surface premelting phenomena in α-gallium

A. Rühm,* H. Reichert, W. Donner,† and H. Dosch‡
Max-Planck-Institut für Metallforschung, D-70569 Stuttgart, Germany

Ch. Grütter and J. Bilgram
Laboratorium für Festkörperphysik, ETH, CH-8093 Zürich, Switzerland

(Received 25 April 2003; revised manuscript received 23 September 2003; published 30 December 2003)

We present a detailed x-ray study of premelting phenomena in the bulk and at the (100) surface of α-gallium single crystals using conventional and grazing angle diffraction. In the bulk we find anisotropic anomalies of the lattice vibrations and the thermal expansion above onset temperatures of about 20 °C along the [010] direction and 27 °C along the [001] direction. At the melting temperature $T_m = 29.76$ °C the vibrational amplitude along [010] approaches the difference of covalent and metallic bond lengths, which is likely to induce a charge transfer between these bonds. We believe that this is the crucial effect that eventually destabilizes the stacking of metallic (010) bilayers characteristic for α-gallium and initiates the transition to the isotropic liquid phase. We observed no anomalies of the lattice vibrations or the thermal expansion along the [100] direction. At the Ga(100) surface isotropic blocked surface melting sets in simultaneously with the bulk anomalies and appears to be initiated by the bulk disordering. The liquidlike surface layer is found to grow logarithmically with temperature up to a final thickness of about 11 Å. In the presence of this layer, we observe anomalous thermal expansion in an adjacent relaxed subsurface layer.

DOI: 10.1103/PhysRevB.68.224110 PACS number(s): 64.70.Dv, 61.66.Bi, 61.10.Nz, 68.35.−p

I. INTRODUCTION

Melting is an ubiquitous phenomenon in every day life and has been investigated intensively for decades.[1–5] It is well known that the solid-liquid phase transition is a first-order transition and therefore involves a nucleation step. However, despite all the research devoted to melting in the past, it is still not clear how this nucleation is initiated and where the liquid phase nucleates in a crystal. One of the few experimental windows to look into such microscopic details of the melting process is provided by the study of structural melting precursors. We present here a comparative temperature-dependent x-ray study of such precursors in α-gallium that enables us to address many of the related open questions discussed in the following introductory section about premelting phenomena.

A. Premelting phenomena

1. Melting precursors

It is now generally accepted that the actual melting process is accompanied by precursory disordering well below the bulk melting temperature T_m. The most prominent precursors are anomalously enhanced atomic vibrations,[1,6–9] a proliferation of vacancies[10–12] and dislocations,[13–15] an anomalous lattice expansion,[16] and, in particular, surface melting.[9,17–43] A recent overview of this topic is given in Ref. 44. Several premelting phenomena are visualized schematically in Fig. 1. Close to T_m lattice vibrations or the thermal root-mean-squares (r.m.s.) displacements of atoms from their equilibrium lattice position [Fig. 1(a)] are often anomalously enhanced as compared to a linear temperature dependence at lower temperatures. This may be explained for example by anharmonicities of the interatomic potential or a proliferation of vacancies near T_m. At the same time the thermal expansion [Fig. 1(b)] may be anomalously enhanced or reduced due to related, but system dependent phenomena (see below). These precursors may occur both in the bulk of a material and/or near the surface.

During the last twenty years it has become apparent that another precursor, the surface melting phenomenon [Fig. 1(c)], plays a key role in the understanding of the solid-liquid phase transition. Surface melting denotes the breakdown of the crystal structure in a thin surface layer below T_m. At T_m the liquidlike surface layer (in which, however, some crystallinity is still preserved) can then serve as a two-dimensional nucleus for the bulk liquid phase, which can explain why superheating of crystals is very rarely observed. Also for this reason, surface melting has been the most promising candidate in the search for *the* melting precursor that can eventually lead to a microscopic explanation of melting. In thermodynamic terms, surface melting is often expected below T_m as it can slightly reduce the free energy of a crystal surface.[18] The liquidlike layer thickness L increases with temperature until it saturates at a finite value at T_m [see Fig. 1(c)]. According to mean-field theory, this increase is logarithmic [$L \propto -\ln(1-T/T_m)$] if short-range interactions are dominating in the liquidlike layer, and it follows a power law dependence ($L \propto T^{1/3}$) if long-range van der Waals interactions are dominating. Note, however, that the bulk structure is not directly affected until actual bulk melting sets in at T_m.

2. Relations between melting precursors

Despite the large body of experimental evidence about melting precursors, there are still many unanswered questions. In particular, it is still unkown how the different pre-

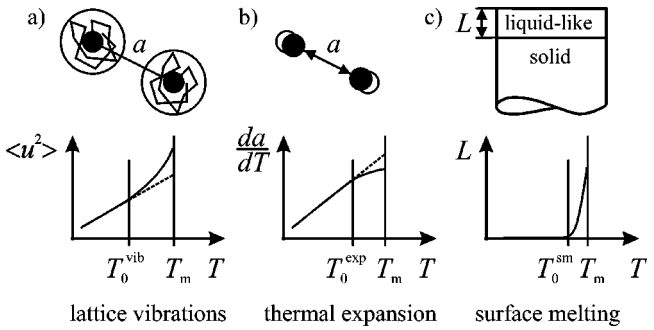

FIG. 1. Commonly observed melting precursors that can arise at different onset temperatures T_0 below T_m. $\langle u^2 \rangle$ denotes the root-mean-squares (r.m.s.) displacements of atoms from their equilibrium lattice position due to thermal motion. a denotes a lattice parameter or a certain interatomic distance. L denotes the thickness of the liquidlike layer in the presence of surface melting.

cursors are related to each other. Note, for example, that an anomalous lattice expansion can be caused by an anharmonicity of the interatomic potential, but also by a proliferation of vacancies and the subsequent lattice relaxation. In either case one would expect the anomalous lattice expansion to be accompanied by anomalously enhanced lattice vibrations: In the first scenario the interatomic potential flatens with increasing temperature, thus allowing for a larger amplitude of atomic motions; in the second scenario the motions of atoms next to a vacancy are geometrically less constrained and therefore enhanced. In most experimental studies, however, such correlations between melting precursors are not investigated or discussed.

Also, while both bulk and surface precursors have been studied intensively but separately in the past, a possible relation between bulk and surface premelting phenomena has never been investigated systematically. Intuitively one may argue that bulk melting should be preceded by surface melting since the strength of interatomic bonds is reduced at most surfaces due to the altered coordination of the atoms. Certain bulk precursors, however, may very well occur before surface melting sets in, in particular precursors that affect the crystallinity only slightly. For example, it was found on Al(110) that surface melting was preceded by an anomalous enhancement of the thermal vibrations in the underlying bulk[21] (in which the long-range crystalline order was still preserved), an observation that was also predicted by earlier molecular dynamics simulations.[45] In this context the question arises of whether precursors that are found in the bulk of a crystal [such as anomalous thermal vibrations in the case of Al(110)] are enhanced or altered at or near the surface. In turn, it is also unclear if an analogon to surface premelting also exists in the bulk, for example, a slight symmetry change of the bulk crystal lattice before the actual transition to the isotropic liquid phase occurs at T_m.

3. Crucial precursors

Finally, apart from the question about relations between different precursor effects, it is also unclear if the eventual discontinuous destabilization of the crystal structure at T_m is actually initiated or *triggered* by a *particular* precursor. It is clear due to Gibbs' phase rule that the liquidlike surface layer in the presence of surface melting cannot evolve into a macroscopic liquid phase even very close to T_m. Lindemann's widely confirmed empirical criterion,[1] on the other hand, claims that a (bulk) crystal becomes unstable when the thermal vibrations of atoms exceed a critical threshold which turns out to be about 7 to 13 % of the nearest-neighbor distance as derived from experimental evidence[5–8] (for a more detailed discussion see Sec. IV F). Similarly, one may expect that a strongly altered thermal expansion can induce a weakening of particular bonds in a crystal that may be crucial for the stability of the lattice. Up to now, however, no detailed comparative study has been performed to elucidate the actual relevance of a particular (bulk or surface) melting precursor for the melting process on an atomic scale.

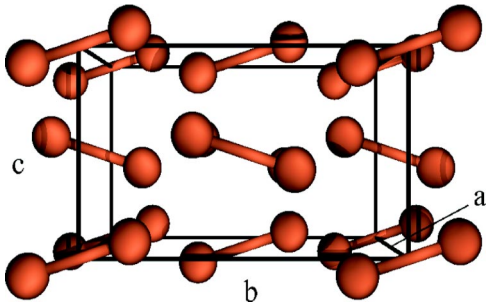

FIG. 2. (Color online) Orthorhombic unit cell of α-gallium. The dimer bonds are indicated as rods connecting pairs of gallium atoms.

B. Gallium

To fill this gap and to attempt an answer to the questions raised above, we present a comparative x-ray study of structural melting precursors (Fig. 1) in α-gallium, a highly anisotropic semimetal that can be regarded as a representative of a class of substances with a complex symmetry and bond character. The most striking feature of α-gallium is the coexistence of metallic and covalent (dimer) bonds that determines many of its unusual physical properties.[5,46] Its orthorhombic unit cell with room temperature lattice parameters $a=(4.519\pm0.001)$ Å, $b=(7.657\pm0.001)$ Å, and $c=(4.526\pm0.001)$ Å (Ref. 46) is depicted in Fig. 2. To investigate how this crystal undergoes melting on the atomic scale in the bulk and at the surface, we employed conventional as well as grazing angle diffraction (GAD) techniques[22] and characterized in detail the temperature dependence of Bragg reflections along various crystal directions.

A highly anisotropic material was selected intentionally for our studies, since one of the most interesting and important aspects of melting is the symmetry change associated with the transition from the crystalline to the isotropic liquid phase. So far most investigations of premelting have been performed on cubic crystals[17,21,47] the symmetry of which is already close to the isotropic symmetry of the melt. Here we focus on a system of lower symmetry to investigate how melting precursors associated with specific crystal directions

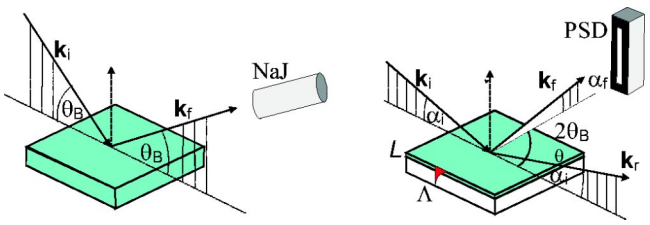

FIG. 3. (Color online) Scattering geometry used for bulk and surface sensitive experiments, respectively. k_i, k_r, and k_f are the wave vectors of the incident, the reflected, and the diffracted beam, respectively, α_i and α_f the incidence and the exit angle, θ_B denotes the Bragg angle, Λ the penetration depth of the x rays, and L the thickness of the liquid-like surface layer. The NaJ scintillation counter and the position-sensitive wire detector (PSD) are also indicated.

affect the stability of the lattice and whether precursory symmetry changes are detectable in the premelting regime.

II. EXPERIMENTAL

Gallium single crystals of high purity were grown in an ultrahigh-vacuum (UHV) environment from the melt using the Nacken-Kryoupolous technique.[48] For the GAD experiments, mirrorlike flat crystal surfaces were prepared by mechanical polishing in a large refrigerator unit providing a cooled environment which was held at temperatures between -20 and 0 °C during the 3 mm diamond polish (approximately 2 h) and between 0 and $+8$ °C during the final Syton polish (0.5–1.5 min). To minimize the mechanical stress on the fairly soft single crystals they were melted into a Tantalum crucible with the back side, and the contact pressure applied to the surface during polishing was held below 100 g/cm^2. According to an STM investigation,[49] the typical surface morphology was characterized by large flat facets, decorated with in some cases fairly large ($\approx$500 Å in diameter, $\approx$60 Å in height), but isolated hillocks. The presence of flat facets ensures that the information depth can be tuned in a well-defined way in the nm range via the angle of incidence.[21]

The GAD experiments were carried out at the BW6 wiggler beamline of the Hamburger Synchrotronstrahlungslabor (HASYLAB) using an x-ray wavelength $\lambda \approx 1.2$ Å, the bulk experiments at a Siemens 18 kW rotating anode using $\lambda \approx 1.54$ Å. During the surface and bulk sensitive experiments the samples were held in a vacuum of about 10^{-9} and 10^{-7} mbar, respectively. Prior to GAD experiments the surfaces were sputter-cleaned with 1 keV Ar^+ ions while the x-ray reflectivity was being monitored simultaneously. Near T_m the sample temperature was controlled with an accuracy of 0.05 K using a cold finger and a thermocouple melted with one side of the sample.

Various Bragg reflections were examined in each scattering mode (see Fig. 3) to characterize the disordering along the three main crystallographic directions [100], [010], and [001] within a temperature range between -150 °C and the melting temperature $T_m = 29.76$ °C. We will discuss bulk and surface disordering separately in the following sections.

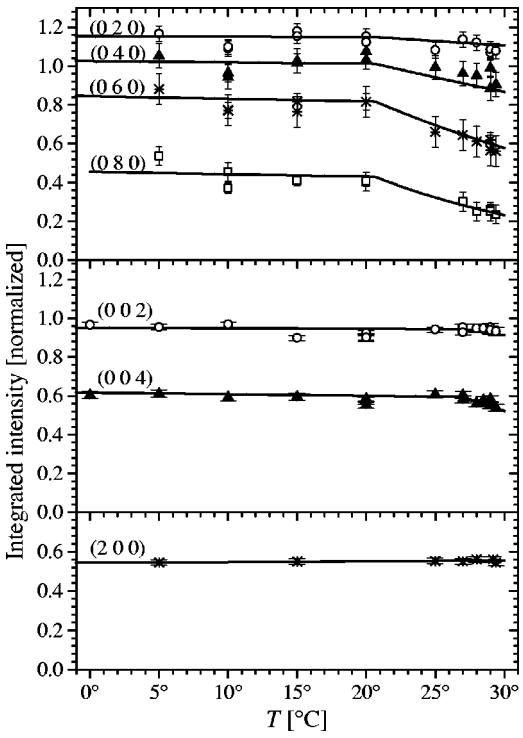

FIG. 4. Temperature dependence of various bulk Debye-Waller factors i_{hkl}. Solid lines represent fits according to the model described in the text.

III. RESULTS

A. Bulk phenomena

In this section we present the results about bulk melting precursors that we obtained by investigating lattice vibrations and thermal expansion on bulk Bragg reflections.

1. Lattice vibrations

When the atoms in a crystal are slightly oscillating around their equilibrium lattice positions due to thermal vibrations, the Bragg intensities of the crystal are reduced and the intensity reduction is given by the so-called Debye-Waller factors[50]

$$i_{hkl} := e^{-\langle (\mathbf{u}\cdot\mathbf{Q}_{hkl})^2 \rangle}, \tag{1}$$

where $\langle (\mathbf{u}\cdot\hat{\mathbf{Q}}_{hkl})^2 \rangle^{1/2}$ is the projection of the root-mean-squares (r.m.s.) displacements $\langle u^2 \rangle^{1/2}$ onto the scattering vector $\mathbf{Q}_{hkl} = |\mathbf{Q}_{hkl}| \cdot \hat{\mathbf{Q}}_{hkl}$. To start with the discussion of our raw data, the temperature dependence of various Debye-Waller factors is plotted in Fig. 4. The Debye-Waller factors i_{hkl} were obtained from the integrated intensity of rocking curves through the respective Bragg reflection (hkl) by correcting for the remaining terms in Eq. (A1) from the Appendix. For the weak (080) reflection the kinematical expression (A2) was used instead. At low temperature ($T \rightarrow 0$ K) the r.m.s. displacements should become small, so all i_{hkl} should approach 1, which is in fair agreement with the experimental data plotted in Fig. 4 (not shown in detail); the remaining

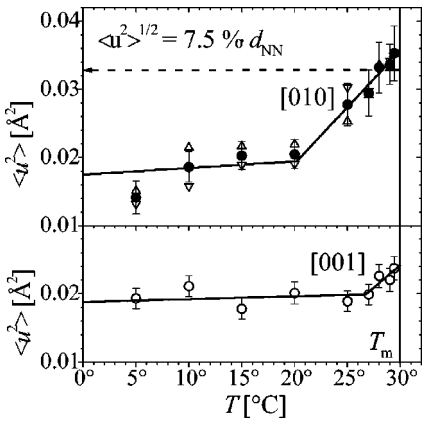

FIG. 5. Root-mean-square displacements of atoms along the main crystallographic directions [010] and [001]. Data points are determined from i_{080} (down triangles), i_{060}/i_{040} (up triangles), the corresponding mean value (filled circles), and i_{004}/i_{002} (open circles). The solid lines represent fits according to the model described in the text.

discrepancies are due to errors in the correction terms applied. With increasing temperature most Bragg intensities decay considerably, especially the higher-order reflections because of the Q dependence of the Debye-Waller factors.

To quantitatively compare the disorder along the [010] and the [001] direction, the corresponding projections of $\langle u^2\rangle$ are plotted versus temperature in Fig. 5. They were derived from the ratios i_{060}/i_{040} and i_{004}/i_{002} in order to minimize the influence of systematic errors, and also directly from i_{080} which is most sensitive to the influence of r.m.s. displacements. Apparently, the results based on i_{060}/i_{040} and i_{080} are consistent with each other (upper panel).

The solid lines in Figs. 4 and 5 represent fits to $\langle u^2(T)\rangle$ which we presumed to grow linearly with temperature T below and above a certain onset temperature T_0 for premelting effects, i.e., $\langle u^2(T)\rangle = \langle u^2(T_0)\rangle + m(T)(T-T_0)$ with constant $m(T)=m_<$ for $T \leqslant T_0$ and $m(T)=m_>$ for $T>T_0$. The low-temperature behavior of the r.m.s. displacements is in accordance with tabulated values for the Debye parameters of α-gallium [from our data and Eq. (A3) from the Appendix we obtain $\Theta_D=(149\pm16)$ K along [010] and $\Theta_D=(238\pm45)$ K along [001]; tabulated values vary considerably: $\Theta_D=(125\cdots240)$ K according to Ref. 51].

At about 20 °C the r.m.s. displacements along [010] start to increase anomalously. This points to considerable anharmonicities of the potential (or a proliferation of vacancies) that become relevant once the r.m.s. displacements exceed 0.14 Å (corresponding to $\langle u^2\rangle = 0.02$ Å^2 in Fig. 5). At the melting temperature T_m, the r.m.s. displacements along [010] reach about 7.5% of the Ga_2 dimer length 2.483 Å (Refs. 46,52) that represents the nearest-neighbor distance in α-gallium. Since the dimers are oriented approximately along [010] with only a slight tilt of 17° (see Fig. 2), our result is semiquantitatively in accordance with Lindemann's criterion which states that a crystalline structure becomes unstable when the thermal vibrations exceed about 7 to 13 % of the nearest-neighbor distance (see Sec. I A 3). In fact, the Lindemann threshold for α-gallium can be quantitatively estimated from thermodynamic parameters to be 4.7% of the nearest-neighbor distance.[7,53,54] This estimation, however, which is based on the assumption of an isotropic monoatomic solid and a harmonic potential energy, does not seem to be exact for α-gallium according to our experimental results. A less significant anharmonic increase of r.m.s. displacements is also observed along the [001] direction at about 27 °C, yet we found no evidence for anomalies along [100] (see lower panel in Fig. 4).

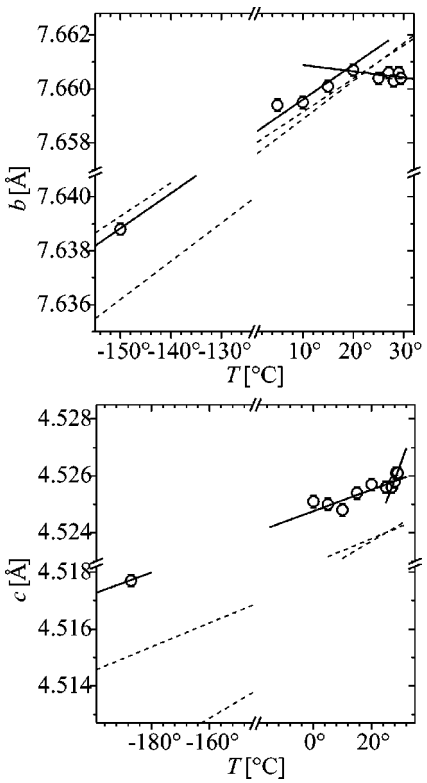

FIG. 6. Temperature dependence of the lattice parameters b and c. The symbols represent mean values of the lattice parameters measured on different Bragg reflections, the solid lines are based on fits according to the model described in the text, and the dashed lines indicate the range of lattice parameters determined from literature data on thermal expansion in α-gallium (Refs. 52,55,73,74). The measured lattice parameter c is slightly offset with respect to the literature values, presumably because of systematic experimental errors.

2. Thermal expansion

As illustrated in Fig. 6, we found the anomalies of the r.m.s. displacements along [010] and [001] to be accompanied by anomalies of the thermal expansion. Assuming a linear temperature dependence of the lattice parameters b and c below and above a certain onset temperature T_0 for premelting effects, we obtain the following fitting results for T_0 and the linear expansion coefficients $\alpha = da/dT$. Along [010]: $\alpha=(16.9\pm0.2)\times10^{-4}$ K^{-1} and $\alpha=(-3.1\pm3.8)\times10^{-4}$ K^{-1} below and above $T_0=(18.0\pm1.9)$ K, respectively. Along [001]: $\alpha=(8.3\pm0.3)\times10^{-4}$ K^{-1} and $\alpha=(61\pm62)\times10^{-4}$ K^{-1} below and above $T_0=(27.9\pm0.9)$ K, respectively. The expansion coefficients measured below T_0 are again consistent with tabulated experimental results

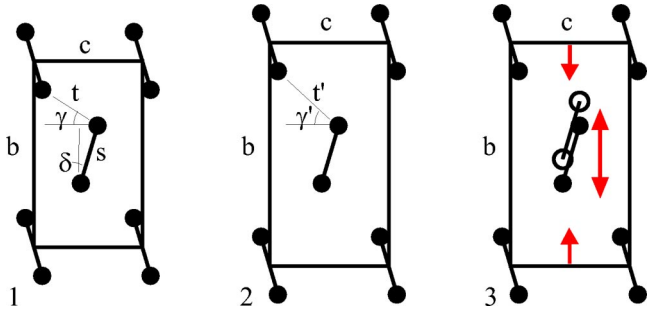

FIG. 7. (Color online) Sketch of possible unit-cell variations within the Ga(100) plane as a consequence of the anisotropic thermal expansion. Stretching of the lattice parameter b and the bond length t $(1\rightarrow 2)$ competes with enhanced dimer vibrations and a related reduction of the expansion along [010] $(1\rightarrow 3)$, with the enhanced vibrations arising from a frustration between two energetically equivalent dimer positions.

(dashed lines in Fig. 6), but the lattice parameter b along [010] stops to increase at about 18 °C. While there is also some evidence for a slightly anomalous increase of the lattice parameter c along [001] at about 28 °C, we observed regular linear thermal expansion along [100] (not shown).

3. Discussion

Before attempting an interpretation of our results, we note that pronounced r.m.s. displacements along [010] at room temperature have also been observed in a crystal-truncation rod scattering study[56] on another α-gallium crystal of similar purity and quality. By contrast, no lattice parameter anomalies have been found in an earlier x-ray investigation on air-grown bulk crystals.[57] We suspect that this discrepancy with our results may be due to impurities in the air-grown crystals.[44]

One possible explanation of the observed bulk anomalies setting in at 18–20 °C could be based on the proliferation of vacancies. For an alternative interpretation, we consider the α-gallium structure as composed of corrugated two-dimensional hexagonal (010) networks.[52,58] Our result that the expansion along [010] stops simultaneously with the anomalous increase of the corresponding r.m.s. displacements could be an indication of local distortions of the regular stacking of (010) networks at elevated temperatures. A schematic illustration of a possible relaxation mechanism is given in Fig. 7, while we point out that the following description is to some extent speculative. The length of the strong dimer bond does not change significantly with temperature,[52] so the anisotropic thermal expansion indicated in Fig. 6 will result in a variation of the bond-length t and the bond angles γ and/or δ (configuration $1\rightarrow 2$). This is energetically unfavorable since bond lengths and bond angles are strongly coupled.[58] Yet, the local bond configuration of at least one of the dimer atoms may be maintained if the dimers are slightly displaced along [010] (configuration 3). The frustration between the two energetically equivalent dimer positions will then give rise to enhanced vibrations of dimers along [010] and to a simultaneous lattice relaxation effecting a reduction of the thermal expansion along [010] as observed in our experiments.

In order to verify this interpretation of our results we propose to look for a charge transfer between bonds of different type (especially those with bond length s and t in Fig. 7) which we expect to accompany the proposed relaxation. In Ref. 58 Häußermann gives a good overview of energetical constraints that determine the lattice geometry in α-gallium, and of the correlations between lattice distortions and the valence electron density distribution in this material. In that context, one might find that the regular thermal expansion below 18–20 °C leads to a successive weakening of the dimer bond and a reduction of its covalent character. The associated increase of the local symmetry of the Ga atoms may eventually be the crucial process initiating the transition to the liquid phase. We emphasize that the r.m.s. displacements at T_m have reached 0.2 Å, which means that the displacements exceed the difference between the nearest-neighbor distance $s=2.483$ Å (the dimer length) and the next-nearest-neighbor distance $t=2.691$ Å. With such a temporary stretching of the dimer bond, however, the distinction between bonds of initially covalent and metallic character, respectively, which determines the unique anisotropic properties of α-gallium, becomes meaningless. In fact, this ought to mark a transition to a more symmetric phase, such as the liquid phase.

B. Surface phenomena

We will now continue with surface precursors in the presentation of our comparative study of premelting effects. We start with a short introduction and then discuss the following surface-related features and properties: the liquidlike layer characteristic for surface melting, lattice vibrations in the still crystalline region near the surface, and finally the thermal expansion in this crystalline near-surface region.

1. Grazing angle diffraction on Ga(100)

For the investigation of surface disordering we chose the Ga(100) surface in our experiments. The selection of this surface orientation was motivated by the strong anisotropy of the physical properties of α-gallium along the two in-plane directions [010] and [001]. This anisotropy can be ascribed to the (approximate) alignment of the Ga_2 dimers along [010] (the tilt angle δ in Fig. 7 is only about 17°). The (100) surface is also distinguished from any other surface by the fact that the tilt angle of dimers against that surface is zero. This situation reflects an intrinsic symmetry condition and may therefore be stable up to T_m. In fact, as reported above, we found no anomalies along [100] in the bulk, so two-dimensional disordering within (100) planes appears to be predominant in the premelting regime. Therefore a GAD investigation of the Ga(100) surface ought to provide fairly exhaustive depth-resolved information about premelting effects along the mainly affected crystal directions in α-gallium.

We have examined various in-plane Bragg reflections along (010) and (001) at an incidence angle $\alpha_i=0.6\alpha_c$, resulting in a penetration depth $l_i=|\mathrm{Im}(k_{i,z})|^{-1}$ of the incident beam of about 50 Å.[22] As an indication of surface melting, a strong intensity reduction of these Bragg reflections is ex-

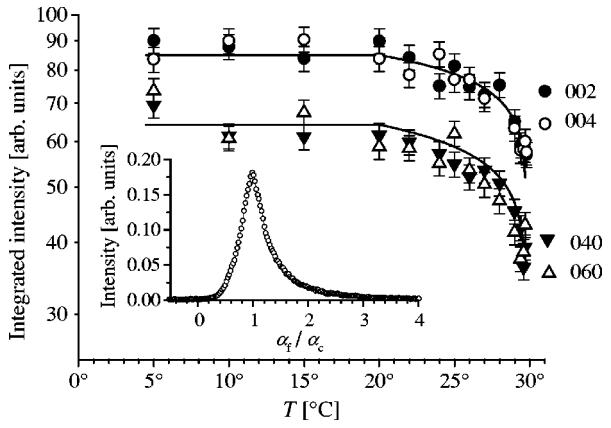

FIG. 8. Temperature dependence of the intensity of various surface Bragg reflections. The data points correspond to integrated intensities of in-plane rocking scans obtained after α_f integration as described in the text. A typical exit-angle profile measured at the (040) reflection is shown in the inset. A detailed line-shape analysis of these profiles [according to Eq. (A4) from the Appendix] revealed that the dynamical scattering theory was applicable even in the near surface region, indicating a high crystalline quality of the large flat terraces on the polished surfaces.

pected once a disordered layer with a thickness of about the scattering depth $\Lambda=(|\mathrm{Im}(k_{i,z})|+|\mathrm{Im}(k_{f,z})|)^{-1}<l_i$ evolves at the surface.[22] To determine the Bragg intensities consistently we recorded exit-angle (α_f) profiles with a position sensitive detector (PSD), as depicted on the right side in Fig. 3, while performing an in-plane rocking scan across the Bragg reflection, i.e., while rotating the sample around the surface normal. In the inset of Fig. 8 we have plotted a typical α_f profile. The actual in-plane rocking scans used to determine the integrated Bragg intensity were obtained by integrating the α_f profiles over a narrow exit-angle interval reaching from 0.93 α_c to 1.07 α_c. According to Eqs. (A4)–(A6) from the Appendix, the integrated intensities plotted in Fig. 8 are thus given by

$$j_{hkl} := \int \int_{0.93\alpha_c}^{1.07\ \alpha_c} \frac{\partial \overline{I}_{hkl}}{\partial \alpha_f}(\omega,\alpha_f)\, d\alpha_f\, d\omega \propto e^{-\langle(\mathbf{u}\cdot\mathbf{Q}_{hkl})^2\rangle} e^{-2L/\Lambda}, \tag{2}$$

where L denotes the thickness of the disordered layer and $\Lambda \approx 43$ Å the scattering depth governed by the incidence and exit angles ($\alpha_i = 0.6\ \alpha_c$, $\alpha_f \approx \alpha_c$).[22] The scattering depth determines the depth range about which information was obtained in the surface sensitive experiments. Note that $\langle u^2\rangle^{1/2}$ has to be interpreted as the r.m.s. displacements of atoms that contribute to the Bragg intensity, i.e., atoms in the crystalline region *below* the disordered layer, not the atoms *within* that layer.

2. Liquidlike layer and near surface lattice vibrations

In contrast to the bulk data shown in Fig. 4, the pronounced intensity decrease of the surface Bragg reflections near T_m is essentially independent of the reflection order (see Fig. 8). This is a direct indication of the evolution of a disordered layer at the surface since the respective damping

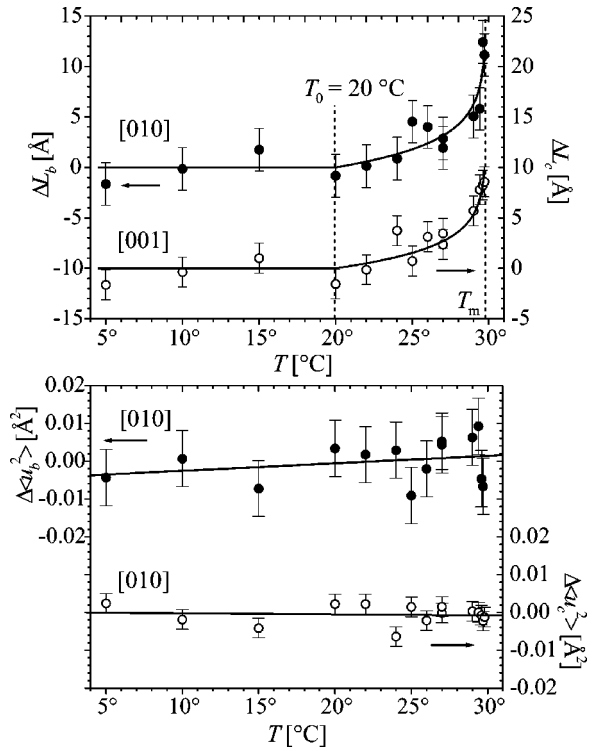

FIG. 9. Temperature dependence of the thickness of the disordered layer and of the r.m.s. displacements as obtained from (0h0) and (00h) reflections according to Eq. (2) (actually calculated from the intensity ratios i_{040}/i_{060} and i_{002}/i_{004} as for the bulk data). The plotted changes ΔL and $\Delta\langle u^2\rangle$ include temperature-independent offsets.

factor $e^{-2L/\Lambda}$ in Eq. (2) does also not depend on Q_{hkl}. The temperature dependence of the two types of disordering considered in Eq. (2), i.e., the evolution of a liquidlike layer at the surface and lattice vibrations in the crystalline region underneath, may be extracted separately from our experimental data, e.g., by plotting $\ln j_{hkl}$ versus Q_{hkl} at each temperature. Due to the complicated influence of the surface morphology and various experimental details (such as the surface miscut, the surface roughness, the sample alignment, as well as the intensity distribution in the primary beam) on the absolute intensity of a surface Bragg reflection, only the changes of L and $\langle u^2\rangle$ with temperature could be determined with high accuracy, but not the absolute values of these quantities. Therefore we plot in Fig. 9 the changes ΔL and $\Delta\langle u^2\rangle$ which include more or less arbitrary but temperature-independent offsets. Nevertheless it is apparent from these data that a disordered surface layer starts to grow at 20 °C, which is exactly the temperature we have already identified above as the onset temperature of various bulk anomalies. The r.m.s displacements, however, do not show any anomalies.

3. Discussion of the liquidlike layer thickness

The temperature dependence of the disordered layer thickness L plotted in the upper panel of Fig. 9 is consistent with a logarithmic growth law as predicted by the mean-field theory of Lipowsky.[18] The growth of L stops at (11 ± 2) Å or

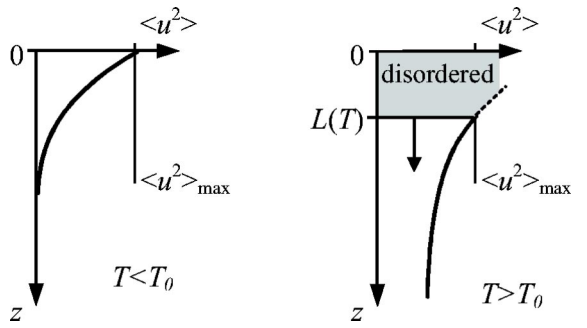

FIG. 10. Model profiles of r.m.s. displacements as a function of depth for temperatures below and above the onset temperature $T_0 = 20\,^{\circ}\mathrm{C}$ of surface melting.

about seven disordered atomic layers at T_m, i.e., we find blocked melting of the Ga(100) surface. This observation corresponds with a recent ellipsometry study[59] in the examined temperature range and may be directly related to the fact that the conductance of liquid gallium is higher than that of the solid phase.[4,18] We did not find a marked difference of the disordering along different in-plane directions (here [010] and [001]) as it was once suggested by an EXAFS study on the Al(110) surface.[47] More recent studies indicate, however, that the crystal morphology in the surface melting regime is likely to be characterized by ordered two-dimensional clusters of atoms,[60,61] which indeed favors a basically isotropic disordering within and below the quasiliquid surface layer.

4. Discussion of the near surface lattice vibrations

Surprisingly, in contrast to the bulk results, the r.m.s. displacements displayed in the lower panel of Fig. 9 do not show any significant anomalies in the examined temperature range. A possible explanation for this result becomes evident from Fig. 10. We argue that below the onset of surface melting (left panel in Fig. 10) $\langle u^2 \rangle$ along [010] grows consistently with temperature at the surface and in the bulk, but that $\langle u^2 \rangle$ is higher at the surface.[62] This corresponds well with studies according to which the displacements of surface atoms exceed the ones of bulk atoms by a factor 1.5 to 2.[9,63–65] Once a critical threshold value $\langle u^2 \rangle_{\max}$ is reached (see Sec. IV F for a more detailed discussion) surface melting sets in. From that temperature on, the value of $\langle u^2 \rangle$ right at the interface between the disordered layer and the crystal below (horizontal line in Fig. 10) remains constant at $\langle u^2 \rangle_{\max}$ while the thickness $L(T)$ of the disordered layer increases. A slight further increase of the value of $\langle u^2 \rangle$ with temperature in the surface-related experimental data (lower panel in Fig. 9) may be due to the fact that the profile of $\langle u^2 \rangle$ as a function of depth z over which the surface sensitive x-ray measurements integrate changes slightly as the r.m.s. displacements in the bulk becomes more pronounced (see right panel in Fig. 10).

5. Thermal expansion

Roughly simultaneously with the onset of surface melting at 20 °C, we observe anomalies of the thermal expansion in the crystalline subsurface region that are even more pronounced than in the bulk (see Fig. 11). The lattice parameter b even shrinks above 25 °C rather than becoming basically constant as in the bulk. The lattice parameter c starts to increase anomalously at 22 °C, while in the bulk such a behavior was only observed above 27 °C. We believe that the enhanced anomalies of the thermal expansion as compared to the bulk are due to the fact that the liquidlike layer cannot exert coherence forces on the underlying crystalline region. It is likely that dislocations are present within or underneath the crystalline subsurface region to allow for the slight discrepancies with the bulk lattice parameters.

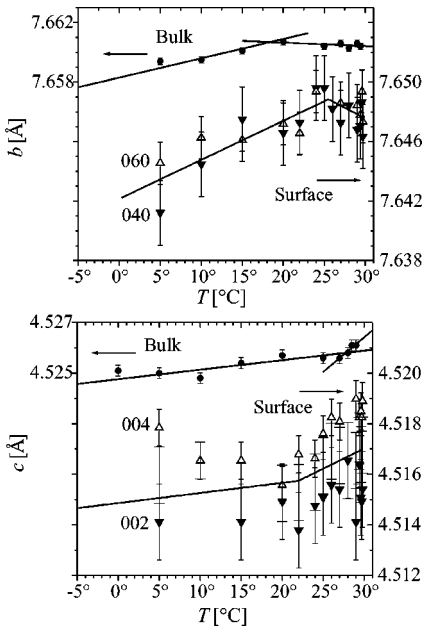

FIG. 11. Temperature dependence of the lattice parameters b and c as determined from various Bragg reflections in GAD geometry. The solid lines again represent fits to the data as in the bulk case. The discrepancy of the surface thermal expansion along [010] with reference to the bulk data below 20 °C is not significant since data points at low temperatures (below −150 °C, not shown in our figures, but included in the fits) are missing in this case.

IV. DISCUSSION

A. Summary of the observed precursor effects

We now summarize all results in terms of the scenario depicted in Fig. 12 which shows a depth profile of melting precursors near the Ga(100) surface as a function of temperature. We found that surface melting sets in at 20 °C simultaneously with anomalies of the thermal expansion and the lattice vibrations along [010] in the bulk. The observation of blocked surface melting at the Ga(100) surface, characterized by a logarithmic growth of the liquidlike layer thickness up to 11 Å at T_m, is in accordance with theoretical expectations (see Sec. III B 3). No significant in-plane anisotropy of the layer thickness was observed, i.e., Fourier components along [010] and [001] disappear in the same manner when approaching T_m.

Upon further heating above 20 °C, a relaxed, still crystalline subsurface layer of presumably several 10 Å thickness

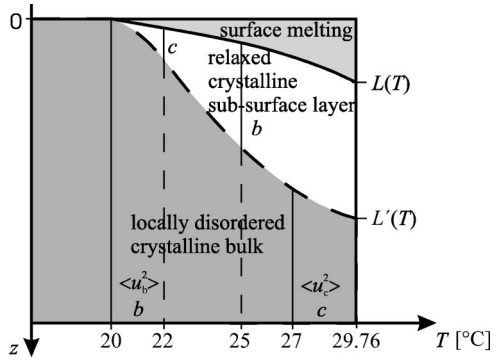

FIG. 12. Schematic illustration of the depth profile of melting precursors as a function of temperature. In each regime the variables showing anomalies are noted. Furthermore, the thickness $L(T)$ of the disordered layer is indicated.

$[L'(T)$ in Fig. 12] develops. This subsurface layer is characterized by an anomalous thermal expansion along [010] and [001] as well as near-critical lattice vibrations. One might speculate that the enhanced (coherent) lattice relaxation in that subsurface region is due to a modified stress and strain scenario right below the disordered layer which cannot exert coherence forces on the subsurface layer. This can to some extent be related to molecular dynamics simulations on simple model systems.[45,61] At 27 °C the bulk (in a depth of the order of microns below the surface) also develops slight anomalies along the [001] direction, both in the thermal expansion and the lattice vibrations.

At the melting temperature $T_m = 29.76$ °C the amplitude of the lattice vibrations along [010] in the bulk approaches 0.2 Å and thus exceeds the difference of covalent and metallic bond lengths (s and t in Fig. 7, respectively). We believe that this induces a charge transfer between these different types of bonds, and that this is the crucial process that actually destabilizes the stacking of metallic (010) bilayers in the crystalline α-gallium phase at T_m. In that sense, bulk melting does not seem to be triggered microscopically by surface melting. It rather seems that surface melting is a consequence of the onset of strong bulk anomalies at 20 °C.

For completeness, we mention that in our experiments we did not observe a linebroadening of Bragg reflections, which indicates that the dislocation density and the coherence length of the crystals did not change drastically with temperature. As far as the surface sensitive measurements are concerned, this argument is for geometrical reasons restricted to dislocations with a Burgers vector parallel to the surface and a dislocation line perpendicular to the surface. On the basis of our data, we will now attempt to give answers to the various questions addressed in Sec. I A for the case of α-gallium.

B. Relations between bulk precursors

At 20 °C we found clear evidence for a relation between anomalies of the lattice vibrations and the thermal expansion along [010] in the bulk. Such a relation can be based on a proliferation of vacancies or on anharmonicities of the interatomic potential and can thus be expected as mentioned in Sec. I A. For a microscopic understanding we have also introduced and discussed a specific model for α-gallium in Fig. 7. At 27 °C a similar but less significant correlation between lattice vibrations and the thermal expansion was found along [001]. Without further detailed and quantitative understanding of the atomic and electronic structure of α-gallium, however, at present no connection can be established between precursors found in the [010] and the [001] direction, respectively.

C. Relations between surface precursors

The disordering at the Ga(100) surface occurs simultaneously and equivalently along [010] and [001], indicating that surface melting is isotropic. Other than that, no direct relation between different near-surface melting precursors becomes evident from our data. However, we have described in which way the onset of surface melting seems to be responsible for the lack of anomalies of the lattice vibrations near the surface: once a critical value of the r.m.s. displacements is exceeded the crystal lattice in the affected region breaks down and does not contribute to the Bragg signal anymore (see Fig. 10). Qualitatively it is also plausible that the thermal expansion is found to be strongly altered in a region directly below the disordered surface layer evolving above 20 °C, because that surface layer does not exert coherence forces on the crystal underneath.

D. Relations between bulk and surface premelting

A connection can also be established between bulk and surface premelting at 20 °C, which is the temperature that marks both the onset of surface melting and of pronounced bulk anomalies along [010] (lattice vibrations and thermal expansion). We suggest two possible interpretations of that connection. First, surface melting may simultaneously affect structural properties of the bulk crystal by means of long-range forces. The range of such forces, however, can hardly extend into the micron range which represents the depth sensitivity of our bulk sensitive experiments. Therefore we do not favor this interpretation. Second, the bulk anomalies may be due to the proliferation of vacancies, anharmonicities of the inter-atomic potential, electronic effects such as a charge transfer between bonds of different type, or a combination of such effects. As soon as these effects manifest themselves in anomalies of the bulk structure, the surface melts due to the altered coordination of surface atoms and the accordingly reduced bond strength. In this case, surface melting would be a consequence of an enhanced manifestation of bulk premelting effects, a scenario that is also suggested in Ref. 9. As indicated in the summary of our observations (Sec. IV A), we strongly favor this second interpretation. Further implications of this are discussed in Sec. IV F.

E. Near surface precursors and bulk symmetry changes

When comparing specific bulk precursors with their near-surface analogon we find quite pronounced differences. The near-surface anomalies of the thermal expansion in the relaxed subsurface layer, for instance, are only qualitatively

similar to the bulk, but they occur at different temperatures and even the sequence of the anomalies along [010] and [001] as a function of temperature is reversed compared to the bulk (see Figs. 6 and 11). The temperature dependence of the near-surface r.m.s. displacements is even qualitatively different from the bulk (see Figs. 5 and 9, lower panel). These observations indicate that there is no simple quantitative relation between bulk and near-surface premelting. We believe that the modified stress and strain scenario in the near-surface region plays an important role in this context and is responsible for the differences in the temperature dependence of melting precursors in the bulk and near the surface.

Likewise, the surface melting precursor does not have a simple analogon in the bulk. While a liquidlike layer develops at the surface, we did not find a simultaneous symmetry change of the unit cell in the bulk as compared to the low-temperature structure (space group *Cmca*).[66]

F. Crucial precursors

It remains to discuss whether there is a specific crucial precursor initiating the melting process, a question that has already been addressed in some of the preceding subsections. The most prominent premelting effects we observed are surface melting and the high final bulk value of the r.m.s. displacements at T_m. Since we observe blocked melting at the Ga(100) surface, the liquid phase is not likely to *preferentially* nucleate at this surface. It might, however, easily nucleate at other surfaces or at edges and corners of the sample which was sometimes observed optically on our samples at the end of an experiment. In any case, it is nowadays widely accepted that the macroscopic liquid phase nucleates at the surface, i.e., especially at high-index surfaces.[63,67] It then remains to explain our experimental observation that along [010] the bulk r.m.s. displacements amount to 7.5% of the nearest-neighbor distance at T_m, which seems to be so well in agreement with the semiquantitative Lindemann criterion according to which the r.m.s. displacements are about 7 to 13 % of the nearest-neighbor distance at T_m.

According to a recent molecular dynamics study on a Lennard-Jones crystal,[9] r.m.s. displacements of 7 to 13 % of the nearest-neighbor distance are actually *not* yet crucial for the stability of a surface-free crystal. Homogeneous nucleation of the liquid phase in the form of so-called Lindemann particles in the bulk does not occur before the *actually* critical value of 22% is reached at the limit of superheating. With the surface r.m.s. displacements being enhanced by a factor of 1.5–2,[9,63–65] however, this critical value of 22% is reached at the surface already at T_m, the equilibrium melting temperature.[9] At T_m heterogeneous nucleation of the melt can set in at the quasiliquid embryo of the liquid phase at the surface. Thus, the quantitative relation between surface and bulk vibrations explains why the empirical Lindemann criterion for equilibrium melting predicts melting already for (in principle noncritical) r.m.s. displacements of 7 to 13 % of the nearest-neighbor distance. These arguments, however, do not yet reveal the actual mechanism for melting.

Although our results are consistent with such general semiquantitative considerations, their implications go beyond these considerations for the case of α-gallium. We found experimentally that at T_m different types of bonds become equivalent. From that we can identify a melting mechanism based on an electronic effect. We argue that the complex bond configuration in α-gallium is destabilized by lattice distortions in connection with a charge transfer between different types of bonds. The presence of such an unusual melting mechanism may also explain the unusually low melting temperature of α-gallium. We believe that this mechanism which may trigger or at least be related to all other observed effects occurring at 20 °C (the anomalies of the r.m.s. displacements in the bulk, the anomalies of the thermal expansion in the bulk and at the surface, as well as surface melting) is perhaps not universal but also crucial for the stability of other substances with a similar bond scenario. It presumably originates from an anharmonicity of the potential energy in α-gallium. Moreover, we expect that the proposed charge transfer between bonds is associated with modified electronic properties. In fact, differences between bulk and surface electronic properties were found in a photoemission and LEED study on Ga(010),[68] which might be an indication of surface melting at this surface.

V. CONCLUSION

In accordance with other work[9,63–65] and with the fact that the coordination of atoms is altered at the surface, we believe that below 20 °C the thermal vibrations at the (100) surface of α-gallium are higher than in the bulk (approximately by a factor of 1.5–2), even though we are not able to derive absolute numbers for the surface vibrations from our surface sensitive x-ray data. At 20 °C anharmonicities of the potential energy manifest themselves in the simultaneous onset of various structural melting precursors (anomalies of the r.m.s. displacements in the bulk, anomalies of the thermal expansion in the bulk and near the surface, as well as surface melting). We believe that a successive charge transfer between different types of bonds is also initiated at that temperature. Due to the altered coordination of surface atoms, the (100) surface starts to melt at 20 °C while the bulk is still stable. While the melting precursors are getting more pronounced with increasing temperature, the crystalline order near the Ga(100) surface is successively destroyed, with the disordered layer thickness reaching (11 ± 2) Å or about seven disordered atomic layers at the melting temperature T_m. At T_m the bulk crystal becomes metastable against homogeneous melting and starts to melt from the liquidlike nuclei at the surface, i.e., especially from high-index surfaces.[63,67] A number of mechanisms have been discussed that can be responsible for the destabilization of the crystal.[9] For the case of α-gallium we conclude from the measured bulk r.m.s. displacements that the crucial mechanism is a charge transfer between different types of bonds that is initiated at 20 °C due to anharmonicities of the potential energy. The charge transfer is complete at T_m, where the r.m.s. displacements along [010] have reached the difference of covalent and metallic bond lengths.

ACKNOWLEDGMENTS

This work was supported by DFG under Contract No. DO352/7-1 and -2. We are indebted to HASYLAB for the hospitality during the experiments. This work was supported by the Swiss National Science Foundation.

APPENDIX

The measured x-ray intensity integrated over a so-called rocking-scan in which the sample is rotated through the (hkl) Bragg reflection is given by[50,69]

$$\int \overline{I}_{\mathrm{det}}(\omega)d\omega = I_0 \frac{8}{3\pi} \frac{r_e \lambda^2 |F_{hkl}| e^{-M} P}{V_c \sin 2\theta_B} \tag{A1}$$

and

$$\int \overline{I}_{\mathrm{det}}(\omega)d\omega = I_0 \frac{1}{2\mu} \frac{r_e^2 \lambda^3 |F_{hkl}|^2 e^{-2M} P}{V_c^2 \sin 2\theta_B} \tag{A2}$$

in the dynamical and kinematical case, respectively. I_0 denotes the intensity measured in the incident beam, μ the linear absorption coefficient, $r_e = 2.818 \times 10^{-15}$ m the classical electron radius, λ the x-ray wavelength, F_{hkl} and V_c the structure factor and the volume of the unit cell, respectively, and θ_B the Bragg angle. $P=1$ or $P=|\cos\theta_B|$ for polarization perpendicular to and within the scattering plane, respectively, and $M = \frac{1}{2}\langle(\mathbf{u}\cdot\mathbf{Q}_{hkl})^2\rangle$. The r.m.s. displacements $\langle u^2\rangle$ are related to the Debye temperature Θ_D via the approximate equation[50]

$$\langle u^2\rangle \approx \frac{3h^2}{4\pi^2 m k_B}\left(\frac{T}{\Theta_D^2} + \frac{1}{36T}\right). \tag{A3}$$

For grazing angle diffraction, the corresponding expressions for the integrated intensity per unit exit angle are[22,70,71]

$$\int \frac{\partial \overline{I}_{\mathrm{PSD}}}{\partial \alpha_f}(\omega,\alpha_f)d\omega = I_0 \frac{\sigma_f}{H_i \sin^2 2\theta_B} \Phi e^{-\sigma^2 |q_{t,z}|^2} \tag{A4}$$

with[72]

$$\Phi = \left| 8\alpha_i\alpha_f \frac{\kappa_i \kappa_f U_+ U_- \Gamma_i \Gamma_f (\tau_+ - \tau_-)}{U_+ V_- W_+ - U_- V_+ W_-} \right|^2 \tag{A5}$$

and[22]

$$\Phi = \frac{r_e^2 \lambda^2 |F_{hkl}|^2 e^{-2M} P}{V_c^2} |T_i|^2 |T_f|^2 \frac{e^{-2L/\Lambda}}{|q_{t,z}|^2} \tag{A6}$$

in the dynamical and kinematical case, respectively. α_i and α_f are the incidence and exit angle, respectively, T_i and T_f are the corresponding transmission functions, Λ is the scattering depth, and $q_{t,z}$ the component of the momentum transfer perpendicular to the surface. H_i is the height of the incident beam, σ_f the width of the exit beam as defined by the detector slits, σ the surface roughness, and L the thickness of the disordered surface layer. The remaining quantities are defined by the following equations:

$$\chi_0 = -2\delta + 2i\beta, \quad \chi_H = -r_e \lambda^2 \frac{F_{hkl}}{\pi V_c},$$

$$\kappa_{i,f} = \sqrt{\chi_0 + \alpha_{i,f}^2},$$

$$\Gamma_{i,f} = e^{ik\kappa_{i,f}L},$$

$$C = e^{-M} \quad \text{and} \quad C = e^{-M}\cos 2\theta_B$$

for polarization perpendicular to and within the scattering plane, respectively,

$$U_\pm = \frac{\tau_\pm^2 - (\chi_0 + \alpha_i^2)}{C\chi_{\bar{H}}},$$

$$V_\pm = (\kappa_i + \alpha_i)(\kappa_i + \tau_\pm) - (\kappa_i - \alpha_i)(\kappa_i - \tau_\pm)\Gamma_i^2,$$

$$W_\pm = (\kappa_f + \alpha_f)(\kappa_f + \tau_\pm + \eta) - (\kappa_f - \alpha_f)(\kappa_f - \tau_\pm - \eta)\Gamma_f^2.$$

$\tau_\pm$ are the two of the four solutions of the fundamental equation of the dynamical scattering theory for the two-beam case

$$(\alpha_i^2 + \chi_0 - \tau^2)[\alpha_f^2 + \chi_0 - (\tau + \eta)^2] = C^2 \chi_H \chi_{\bar{H}},$$

that have a positive imaginary part.

*Electronic address: ruehm@mf.mpg.de

†New address: University of Houston, Department of Physics, Houston, Texas 77204, USA.

‡Electronic address: dosch@mf.mpg.de. Also at Universität Stuttgart, Institut für Theoretische und Angewandte Physik, D-70569 Stuttgart, Germany.

[1] F.A. Lindemann, Phys. Z. **11**, 609 (1910).

[2] M. Born, J. Chem. Phys. **7**, 591 (1939).

[3] A.R. Ubbelohde, *Melting and Crystal Structure* (Clarendon Press, Oxford, 1965), and references therein.

[4] J.N. Israelachvili, *Intermolecular and Surface Forces* (Academic Press, San Diego, 1985), and references therein.

[5] J.H. Bilgram, Phys. Rep. **153**, 1 (1987), and references therein.

[6] E. Grüneisen, in *Handbuch der Physik* (Springer, Berlin, 1926), pp. 1–59.

[7] J.J. Gilvary, Phys. Rev. **102**, 308 (1955).

[8] J.J. Gilvary, Phys. Rev. **103**, 1700 (1956).

[9] Z.H. Jin, P. Gumbsch, K. Lu, and E. Ma, Phys. Rev. Lett. **87**, 055703 (2001).

[10] D.K.C. McDonald, J. Chem. Phys. **21**, 177 (1953).

[11] D.K.C. McDonald, W.B. Pearson, and L.T. Toele, Can. J. Phys. **34**, 389 (1956).

[12] L.G. Carpenter, J. Chem. Phys. **21**, 2244 (1953).

[13] D.P. Woodruff, *The Solid-Liquid Interface* (Cambridge University Press, London, 1973), and references therein.

[14] R.M.J. Cotterill, E.J. Jensen, and W.D. Kristensen, in *Anharmonic Lattices, Structural Transitions and Melting*, edited by T. Riste (Nordhoff, Leiden, 1974).

[15] L. Burakovsky, D.L. Preston, and R.R. Silbar, J. Appl. Phys. **88**, 6294 (2000).

[16] R.M. Nicklow and R.A. Young, Phys. Rev. B **129**, 1936 (1963).

[17] J.W.M. Frenken and J.F. van der Veen, Phys. Rev. Lett. **54**, 134

(1985).
[18] R. Lipowsky, Ferroelectrics **73**, 69 (1987).
[19] A.W. Denier v.d. Gon, R.J. Smith, J.M. Gay, D.J. O'Connor, and J.F. v.d. Veen, Surf. Sci. **227**, 143 (1990).
[20] H.M. van Pinxteren and J.W.M. Frenken, Surf. Sci. **275**, 383 (1992).
[21] H. Dosch, T. Höfer, J. Peisl, and R.L. Johnson, Europhys. Lett. **15**, 527 (1991).
[22] H. Dosch, *Critical Phenomena at Surfaces and Interfaces* (Springer, Berlin, 1992), and references therein.
[23] P. von Blankenhagen, W. Schommers, and V. Voegele, J. Vac. Sci. Technol. A **5**, 649 (1987).
[24] A. Pavlovska, M. Tikhov, Y. Gu, and E. Bauer, Surf. Sci. **278**, 303 (1992).
[25] I. Golecki and C. Jaccard, J. Phys. C **11**, 4229 (1978).
[26] M. Elbaum, Phys. Rev. Lett. **67**, 2982 (1991).
[27] A. Lied, H. Dosch, and J.H. Bilgram, Phys. Rev. Lett. **72**, 3554 (1994).
[28] H. Dosch, A. Lied, and J.H. Bilgram, Surf. Sci. **366**, 43 (1996).
[29] M. Elbaum, S.G. Lipson, and J.G. Dash, J. Cryst. Growth **129**, 491 (1993).
[30] Y. Furukawa and H. Nada, in *Advances in the Understanding of Crystal Growth Mechanism*, edited by T. Nishinaga (Elsevier, Amsterdam, 1997).
[31] F. Rieutord, R. Simon, R. Conradt, and P. Müller-Buschbaum, Europhys. Lett. **37**, 565 (1997).
[32] R. G. Silfhout, Ph.D. thesis, University of Leiden, Leiden, 1992.
[33] J. Fraxedas, S. Ferrer, and F. Comin, Europhys. Lett. **25**, 119 (1994).
[34] L. Gavioli, M.G. Betti, and C. Mariani, Phys. Rev. Lett. **77**, 3869 (1996).
[35] B.M. Ocko, D. Gibbs, K.G. Huang, D.M. Zehner, and S.G.J. Mochrie, Phys. Rev. B **44**, 6429 (1991).
[36] G. Bilalbegovic and E. Tosatti, Phys. Rev. B **48**, 11 240 (1993).
[37] A.W. Denier v.d. Gon, J.M. Gay, J.W.M. Frenken, and J.F.v.d. Veen, Surf. Sci. **241**, 335 (1991).
[38] T. Shimizu and T. Yamamoto, J. Chem. Phys. **113**, 3351 (2000).
[39] N. Takeuchi, A. Selloni, and E. Tosatti, Phys. Rev. B **55**, 15 405 (1997).
[40] B. Demirdjian, D. Ferry, J. Suzanne, C. Toubin, S. Picaud, P.N.M. Hoang, and C. Girardet, J. Chem. Phys. **116**, 5143 (2002).
[41] Y. Fukaya and Y. Shigeta, Phys. Rev. B **65**, 195415 (2002).
[42] V. Sadtchenko and G.E. Ewing, J. Chem. Phys. **116**, 4686 (2002).
[43] X. Wei, P.B. Miranda, and Y.R. Shen, Phys. Rev. Lett. **86**, 1554 (2001).
[44] J.G. Dash, Rev. Mod. Phys. **71**, 1737 (1999).
[45] P. Stoltze, J.K. Norskov, and U. Landman, Phys. Rev. Lett. **61**, 440 (1988); Surf. Sci. **220**, L-693 (1989).
[46] A. Defrain, J. Chim. Phys. Phys.-Chim. Biol. **74**, 851 (1977).
[47] M. Polcik, L. Wilde, and J. Haase, Phys. Rev. Lett. **78**, 491 (1997).
[48] H.E. Buckley, *Crystal Growth* (Wiley, New York, 1951).
[49] Ch. Grütter, A. Rühm, J.H. Bilgram, and H. Dosch (unpublished).
[50] B. E. Warren, *X-Ray Diffraction* (Dover, New York, 1990).
[51] *International Tables for X-Ray Crystallography*, 2nd ed., edited by C. MacGillvary and G.D. Rieck (Kynoch Press, Birmingham, 1968), Vol. III, p. 238.
[52] B.D. Sharma and J. Donohue, Z. Kristallogr. **117**, 293 (1962).
[53] We used $v_m = 4.519 \times 7.657 \times 4.526/8$ Å^3 and $r_m = 2.483$ Å to calculate $v_m / r_m^3 = 1.279$ for the α-gallium lattice [see Eq. (8) in Ref. 7].
[54] A. di Cicco and A. Filipponi, Europhys. Lett. **27**, 407 (1994).
[55] b, c at 25 °C from Ref. 52, db/dT and dc/dT from Refs. 73 and 74.
[56] D.A. Walko, I.K. Robinson, Ch. Grütter, and J.H. Bilgram, Phys. Rev. Lett. **81**, 626 (1998).
[57] G. Mair, K. Hamacher, and H. Wenzl, Z. Phys. B **24**, 301 (1976).
[58] U. Häußermann, S.I. Simak, I. Abrikosov, and S. Lidin, Chem.-Eur. J. **3**, 904 (1997).
[59] Ch. Grütter, Ph.D. thesis, ETH Zürich, Zürich, 1997.
[60] L. Pedemonte, G. Bracco, A. Robin, and W. Heiland, Phys. Rev. B **65**, 245406 (2002).
[61] R.L. Davidchack and B.B. Laird, J. Chem. Phys. **108**, 9452 (1998).
[62] Note, however, that we could not actually determine the absolute value of $\langle u^2 \rangle$ from the GAD data as explained in Sec. III B 2.
[63] R.M. Goodman and G.A. Somorjai, J. Chem. Phys. **52**, 6325 (1970).
[64] K. Hoshino and S. Shimamura, Philos. Mag. A **40**, 137 (1979).
[65] R.W. Cahn, Nature (London) **323**, 668 (1986).
[66] *Strukturdaten der Elemente*, Landolt-Börnstein, Neue Serie, Vol. 6, edited by K.-H. Hellwege (Springer, Berlin, 1971).
[67] I.N. Stranski, W. Gans, and H. Rau, Ber. Bunsenges. Phys. Chem. **67**, 965 (1963).
[68] Ph. Hofmann, Y.Q. Cai, Ch. Grütter, and J.H. Bilgram, Phys. Rev. Lett. **81**, 1670 (1998).
[69] W. H. Zachariasen, *Theory of X-Ray Diffraction in Crystals* (Dover, New York, 1994).
[70] S.K. Sinha, E.B. Sirota, S. Garoff, and H.B. Stanley, Phys. Rev. B **38**, 2297 (1988).
[71] A. Rühm, Ph.D. thesis, University of Wuppertal, Wuppertal, 1998.
[72] N. Bernhard, E. Burkel, G. Gompper, H. Metzger, J. Peisl, H. Wagner, and G. Wallner, Z. Phys. B **69**, 303 (1987).
[73] E.I. Geshko and V.P. Michal'chenko, Sov. Phys. Solid State **14**, 1554 (1972).
[74] G. Mair, Ph.D. thesis, University of Innsbruck, Berichte der KFA Jülich, 1975.